nature communications

Article

https://doi.org/10.1038/s41467-025-66634-7

An unfinished Pompeian construction site reveals ancient Roman building technology

Received: 25 March 2025

Accepted: 11 November 2025

Published online: 09 December 2025

Check for updates

Ellie Vaserman[1], James C. Weaver[1], Claire Hayhow[1,2], Kristin Bergmann[1,2], Celestino Grifa[3,4], Roberto Scalesse[5], Valeria Amoretti[6], Antonino Russo[6], Gennaro Iovino[6], Gabriel Zuchtriegel[6] & Admir Masic[1]

Recent excavations at Pompeii's Regio IX have uncovered an intact ancient construction site, offering insights into Roman building techniques at the time of the eruption of Mount Vesuvius in 79 CE. Microstructural and chemical analysis of materials collected from previously constructed walls, walls under construction, and adjacent dry, raw material piles show unequivocally how quicklime was pre-mixed with dry pozzolan before adding water in the creation of Roman concrete. This construction method, also known as hot mixing, results in an exothermic reaction within the mortar and the formation of lime clasts, key contributors to the self-healing and post-pozzolanic reactivity of hydraulic mortars. The analysis of reaction rims around volcanic aggregates demonstrate aggregate/matrix interfacial remodeling, where calcium ions originating from the dissolution of lime clasts diffuse and remineralize, producing amorphous phases and various polymorphs of calcium carbonate (including calcite and aragonite). Furthermore, the parallel discovery of masonry materials and tools permits elucidation of the entire construction workflow, including the steps required to process binding mortars and larger aggregates (caementa). These findings advance our understanding of ancient Roman construction and long-term material evolution, providing a scientific basis for developing more durable and sustainable concretes and restoration materials inspired by ancient practices.

Ancient Roman construction strategies have long intrigued scholars in a wide range of different fields, from history and archeology, to materials science and engineering. The Roman architectural revolution, underpinned by advancements in concrete technology, led to unprecedented construction achievements and urban planning innovations[1]. For example, the Romans perfected the production of durable, hydraulic concrete (*opus caementicium*) using volcanic ash (pozzolana) and crushed, fired ceramic (cocciopesto), allowing for large, stable structures that could support complex architectural forms, such as arches, vaults, and domes[2]. This architectural flexibility enabled the creation of iconic structures, from the Pantheon, with its vast, unreinforced concrete dome, to extensive road systems stretching over 400,000 kilometers[3].

Despite widespread fascination in terms of their structural complexity and cultural significance, knowledge of the actual construction processes used to create these infrastructural features remains surprisingly limited, due to the scarcity of physical evidence. The discovery of tools and raw materials from these ancient construction sites

[1]Department of Civil and Environmental Engineering, Massachusetts Institute of Technology, 77 Massachusetts Avenue, Cambridge, MA, USA. [2]Department of Earth, Atmospheric and Planetary Sciences, Massachusetts Institute of Technology, 77 Massachusetts Avenue, Cambridge, MA, USA. [3]University of Sannio, Department of Science and Technology, Via de Sanctis snc, Benevento, Italy. [4]SHerIL, Samnium Heritage Innovation Lab, Complesso Ex Battistine, Benevento, Italy. [5]Soc. ERRESSE s.r.l., via Felice Orsini 2, Priverno, LT, Italy. [6]Parco Archeologico di Pompei, via Plinio 26, Pompei, NA, Italy.
e-mail: masic@mit.edu

that are preserved in situ is uncommon, with most sites being fragmentary, containing only isolated lime kilns, slaking pits, or scattered debris layers[4,5]. Most of the current knowledge of Roman construction techniques thus comes from written records. The key historical sources on ancient technologies are the engineers, architects, and historians Vitruvius and Pliny the Elder, who provided in-depth descriptions of the materials and methods involved in Roman wall construction in their works, "De Architectura" and "Naturalis Historia"[6,7]. Vitruvius describes a process of making *opus caementicium*, commonly used in the erection of long-standing walls, and considered a cornerstone of Roman engineering. According to Vitruvius, the production of Roman concrete began with the preparation of lime, which required heating high-purity limestone in kilns to produce quicklime (CaO), which was mixed with water to create slaked lime ($Ca(OH)_2$)[6,8]. This slaked lime served as the primary binder and was combined with pozzolanic components, primarily composed of silica and alumina-containing minerals (including, for example, pyroclastic rocks and volcanic ash)[9,10].

The mixture of lime and pozzolan was applied in layers within formworks that defined the wall's structure and provided support during the initial setting phase, with each layer embedding large aggregates (*caementa*) such as broken stones or ceramic fragments, which provided resistance to cracking[6–8,11]. In the presence of water and lime, this mixture forms calcium aluminum silicate hydrates (C-A-S-H) through pozzolanic reactions, which are responsible for the material's long-term strength and durability[8,12–17].

Research into the long-term durability of Roman concrete has often focused on the potential impact of ongoing post-pozzolanic reactions that occur long after the initial material was cast[12,18,19]. In marine environments, for example, a multistage mineral evolution has been suggested that includes the dissolution of lime and vitric tuff clasts[20]. This dissolution is followed by the precipitation of C-A-S-H phases that form reaction rims around the aggregates, eventually followed by the crystallization, under ambient conditions, of Al-tobermorite, phillipsite, and strätlingite within the matrix and around pozzolanic aggregates[14,21–24]. The sustained post-pozzolanic reactivity of volcanic aggregates, which may continue over centuries, has been proposed to significantly contribute to the exceptional durability of Roman concrete—a research area of ongoing investigation[19,25,26].

Recently, we reported on the potential use of quicklime instead of, or combined with, slaked lime in archeological Roman mortars[15]. Specifically, this research questions the type of lime used, as originally described by Vitruvius. In book II of *De Architectura*, Vitruvius discusses the selection criteria for specific materials and the detailed processes involved in mortar preparation, beginning with "*ea [the lime] erit extincta*," or "the lime is extinguished," which has been interpreted to refer to the production of "*calx extincta*," or slaked lime ($Ca(OH)_2$)[6]. Although Vitruvius provides detailed descriptions of concrete production, these may only reflect the practices of the late Republic, and should not be assumed to be exhaustive or temporally universal.

Based on the limited available evidence of ancient Roman construction processes, it has been suggested that the slaking of lime generally took place at the construction sites themselves, but it is important to note that pits employed for lime slaking and storage are rare in the archeological record[11,27–29]. Evidence of slaked lime being used in masonry mortar is also fairly limited, with a notable example found in *Lex pariete faciendo*, an inscription from 105 BCE in Puteoli detailing the use of "*calx restincta*", interpreted to refer to slaked lime[30]. Other evidence for the use of lime slaking in imperial mortars can be found in the form of lime encrustations on amphorae. While well documented in the literature, these lime-encrusted amphorae occur in limited quantities, and as such, this evidence cannot be considered sufficient to be the sole calcium source for *opus caementicium* mortars, especially in the post-62 CE building phase in Pompeii[11,29]. It is therefore generally accepted that lime was slaked in small quantities in these amphorae for usage in other construction projects, such as in decorative work or flooring[11,28]. In contrast, the "hot mixing" theory posits that quicklime was mixed directly with pozzolanic materials and water, initiating an exothermic reaction that significantly increased the temperature of the mortar mixture, sometimes exceeding 200 °C in localized "hot spots"[15]. This hot mixing process involves the hydration of quicklime, which can be represented by Eq. (1).

$$CaO + H_2O \rightarrow Ca(OH)_2 + \text{heat} \quad (1)$$

The elevated temperatures and subsequent rapid cooling influence the microstructural development of the mortar, particularly around the lime particles, where the low-humidity conditions prevent their dissolution[15,28]. This process results in the preservation of white lime inclusions, or "lime clasts," in the mortar matrix, which have been linked to the durability and self-healing properties of Roman concrete[15,27]. These undissolved clasts retain a reactive calcium-rich core, that when exposed to water serve as a mobile calcium source that slowly dissolves into the crack and pore network within the matrix. It has been proposed that this calcium-rich solution reacts with pozzolanic material to form additional C-A-S-H phases, and recrystallizes in the form of various polymorphs of calcium carbonate within cracks and pores during natural wetting and drying cycles, effectively functioning as a crack-filling mechanism[15].

While supported through modern research efforts focused on both the analysis of ancient Roman concretes and the behavior of their Roman-inspired modern concrete analogs[15], this hot mixing theory and the historical usage of quicklime depart from Vitruvius' descriptions and suggest alternative or complementary methods may have been in use in 79 CE, highlighting a knowledge gap in our understanding of Roman construction techniques. Furthermore, recent excavations and analyses, such as those at Augusta Raurica in Switzerland, have uncovered mortar mixing pits with partially slaked residues, interpreted as evidence for hot mixing practices in larger-scale Roman construction[31]. While there are some historical descriptions (wall paintings and mosaics) depicting ancient Roman construction practices, there is a general lack of well-preserved and dated physical evidence related to these techniques that persist to the modern day, especially in smaller, domestic projects.

Stores of building materials, which are typical features of construction sites, have been historically difficult to identify in the archeological record and are thus scantily described in the literature[11]. In contrast, the eruption of Mount Vesuvius in 79 CE completely buried the city of Pompeii in pumice lapilli and volcanic ash, allowing modern excavations to recover the daily activities of an ancient Roman city that have been literally frozen in time. Because of the nature of the volcanic deposits that buried Pompeii, the archeological layers are clearly distinguishable from the volcanic ones, and the latter also keep the former in a stable state, immobilized and sealed, preserving the archeological evidence from post-eruptive disturbances. Recent research on mortars from Pompeii has advanced significantly through the use of interdisciplinary and multi-scale characterization approaches, deepening our understanding of materials selection and construction logistics in this ancient Roman city. These analytical investigations have revealed a diverse use of raw materials, including locally collected volcanic ash and pozzolans, and have characterized both original Roman mortars and later restoration phases[32–35]. Statistical and mineralogical analyses, such as discriminant and principal component analysis, have further enabled researchers to differentiate between construction periods, identify technological choices, and trace the evolution and diversity of mortar recipes across time and applications (such as structural, decorative, and flooring mortars)[36–38]. Prior to the eruption, Pompeii experienced significant seismic activity, particularly an earthquake in 62 CE that caused widespread damage across the city[39]. This earthquake led to a period of extensive

https://doi.org/10.1038/s41467-025-66634-7

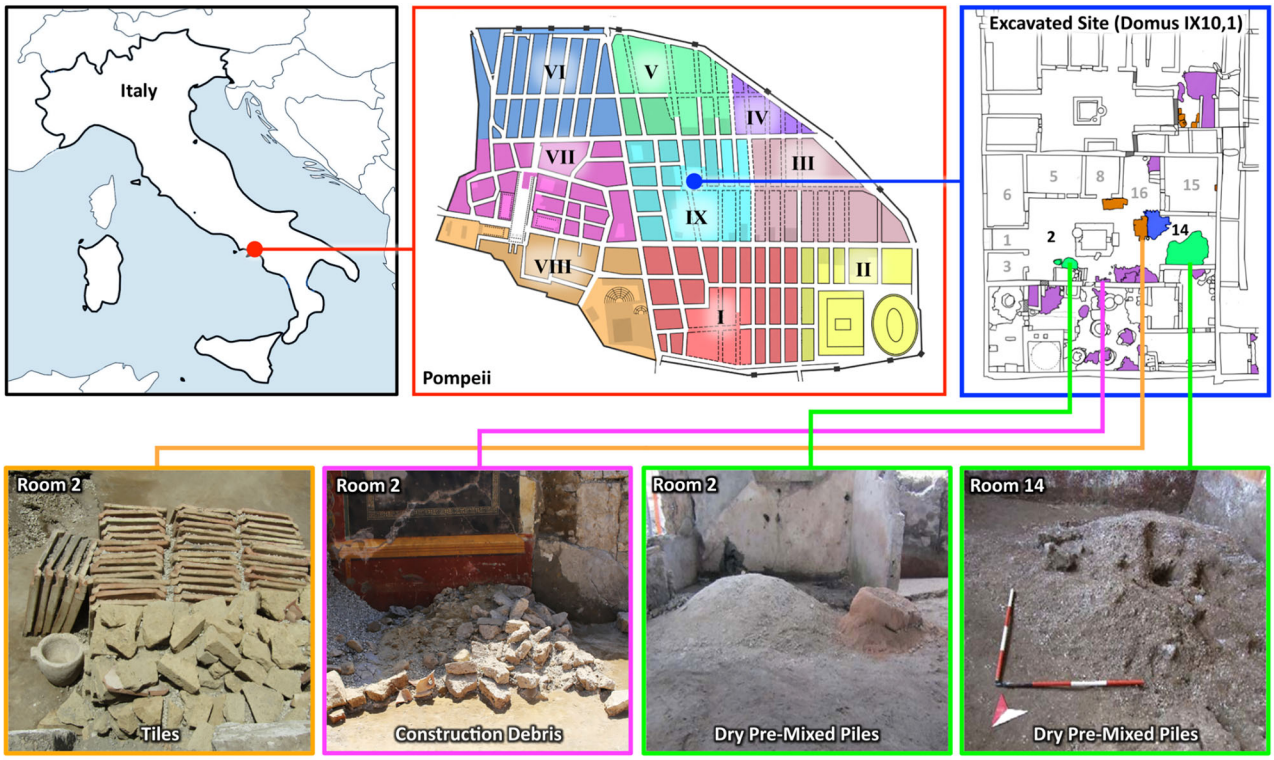

Fig. 1 | Pompeii Archeological Park site map, with *Regio* IX denoted in light blue (upper, middle) and *Domus* IX 10, 1 shown in additional detail, with color-coded piles of raw construction materials (right): purple: debris; green: piles of dry pre-mixed materials; blue: piles of tuff blocks. The excavations have revealed numerous accumulations of demolished and stacked building materials consisting of lava and limestone rubble, tile fragments, and pieces of common ceramics and amphorae, set aside for reuse in the ongoing (first century CE) restoration work on the walls. The two main rooms of *Domus* IX 10, 1 where raw materials were collected for analysis (Rooms 2 and 14) are labeled with black numbers, while the numbers of adjacent rooms are labeled in light gray.

reconstruction, during which many buildings were under-documented stages of repair and renovation[35,40]. The renovations often involved reinforcing structures, updating architectural elements, and repairing decorative features[38,41]. Though some evidence of ancient building activities in Pompeii has been discovered and documented, these investigations have rarely focused on materials characterization or aimed to reconstruct the practical techniques and operations involved in Roman mortar preparation[4,5].

In this paper, we report on the discovery of *Domus IX 10, 1*, a well-preserved active Roman construction site in Pompeii (immediately preceding the eruption of Mount Vesuvius), allowing a unique opportunity for the in-field documentation of important details regarding the associated materials, tools, and construction processes employed (Fig. 1, Supplementary Fig. 1). Specifically, the process for making Roman concrete has been elucidated through these new archeological findings and via targeted materials characterization approaches. Additionally, an in-depth investigation of the reaction rims around the pumiceous vitric aggregates in these cementitious materials provides insights into post-pozzolanic reaction mechanisms. The excavation and exploration of this ancient construction site, which contains raw, unprocessed materials, not only allows the precise reconstruction of ancient technologies but also the development of compatible restoration mortars and the comprehensive integration of historical knowledge.

Results

Evidence of construction activities

Excavations in Pompeii's *Regio* IX *Insula* 10 have provided valuable insights into the nature of ancient construction practices, and the scale and organization of the renovation efforts following the catastrophic earthquake of 62 CE. This series of residential construction projects, designed to stabilize and improve various structures in the vicinity, included raw material production areas and provided strong evidence for systematic resource management and material reuse.

The excavated rooms revealed numerous stacks of recycled building materials, including lava stones, limestone, tile fragments, and pieces of common ceramics and amphorae, all carefully set aside for reuse in ongoing masonry work (see Fig. 1: tiles in orange, residual material in purple, inert material piles in green, and tuff block stacks in blue). Additional building materials were identified in rooms 7 and 16, the latter located at the base of the stairs to the upper floor. The collection and arrangement of these archeological finds support the conclusion that this area served as an active construction site, where raw materials and tools were stored and systematically used (see Supplemental Materials for further details). Construction marks on walls, including sequences of numerals and symbols (Supplementary Fig. 2), may have served as reference points for work schedules, material quantities, or budgeting, providing rare evidence of project management practices in the ancient Roman building industry. In Room 5, several key artifacts were also uncovered, including a lead weight and iron tools such as an ax (Supplementary Fig. 3). The lead weight was medium-sized and conical, retaining an iron handle for suspension, a design consistent with counterweights for balance scales at the time. This discovery suggests its possible use in the precise measuring of material ratios, which would be required to create consistent cement and mortar formulations during the construction process. Room 13 contained additional work tools, both on a masonry bench along the northern wall and on the floor. Smaller items were also found along with nails and mineralized wood fragments, supporting that the objects were all likely stored in a wooden box. Notably, these objects included two plumb bobs, one bronze and the other iron. The

bronze plumb bob exhibited concentric ring decorations and a knob with a hole for a string, suggesting its use in marking verticals, an important task in the erection of walls. The iron plumb bob included a small goat horn that was likely used as a spool for suspending the weight. These tools are indicative of precise construction practices likely used by skilled laborers, essential for the correct alignment of architectural elements. Among the tools was a small chisel with two cutting edges perpendicular to each other, used for cutting stones like tuff, pointing to active stone working at the site.

Aside from tools, other significant evidence of construction activities could be inferred from the variety of piles and stacks of materials. Tile fragments were concentrated in room 28. In the northeast corner, a stack of fragmented tiles was laid atop other stones, suggesting that these tiles were being sorted and prepared for reuse (Fig. 1, Supplementary Fig. 2). These tiles were likely used in the restoration of the roofing or flooring, and the careful stacking and organization of the tiles suggest workers were systematically organizing these materials. Another significant find was the presence of Neapolitan Yellow tuff in various locations throughout *Domus* 1, particularly in room 2 (the *atrium*) and near room 14 (the *tablinum*). The tuff was specifically imported for use in critical concrete structural elements, such as doorposts, corners, and arches. The strategic placement of this tuff in the house suggests that it was likely earmarked for specific structural repairs or enhancements, particularly in load-bearing areas that required the strength and durability of this imported stone. In room 2, a stacked pile of parallelepiped tuff blocks and orderly rows of roof tiles (*imbrex*) were also discovered (Fig.1). Next to the tuff blocks, was a work area containing small-sized chips of tuff stone, the result from rough shaping the square blocks with an ax (*dolabra*) to become facing stones (*caementa)* for the room's wall repairs.

In room 15, three orderly rows of flat roofing tiles (*tegula*), along with three piles of concave roof tiles (*imbrex*), and a corner gutter roofing tile (*collicia*), were also found. These tiles showed clear signs of wear, suggesting that they had been dismantled from existing structures. The careful storage of these tiles suggests that they were intended for reuse, possibly in the reconstruction of the house's roof.

In room 2 (Fig. 1), a pile of pre-mixed materials (consisting of lime and fine and coarse aggregates) together with a pile of *cocciopesto* that showed the imprint of a basket, was found. Most notably, in room 14, there was a large pile of pre-mixed materials with an imprint from a shovel-like tool present (Fig. 1, Supplementary Fig. 4). This pile contained large (several millimeters in size) low-density granules of quicklime, which were dry-mixed with pozzolan and stored for immediate use in the ongoing masonry work. Near this pile, in room 7, the mortar on the wall showed signs of being repaired and reapplied, and a wall between rooms 7 and 13 appeared to be in the process of being constructed (see Supplemental Supplementary Fig. 1). In corridor 10 and courtyard 12, several lime-containing broken amphorae were also found (Supplementary Fig. 5).

Wall construction—a multi-scale characterization analysis

Domus (residential dwelling) 1, in *Insula* (block) 10 of *Regio* (region) IX of Pompeii Archeological Park was excavated in January 2023 (Fig. 1). For this study, samples from this location were collected from a pre-mixed (PM) dry material pile, a newly constructed wall that was being built in 79 CE (W1), a completed buttress wall nearby (W2), a pre-existing structural wall (W3), and mortar repairs in an existing wall (MR). Samples were also collected from additional amphorae and material piles located throughout the interior of the *domus* (see Supplementary Table 1, Supplementary Fig. 1).

To determine the chemical and crystallographic composition of both the pre-mixed material pile (PM) and the walls (MR, W1, W2, and W3), several characterization tools were employed. FTIR-ATR spectra acquired from all of the samples were highly similar and consisted of calcium carbonate and pozzolana, demonstrating uniformity in their basic chemical composition (Supplementary Fig. 6). X-ray diffraction (XRD) conducted on the samples further identified the primary crystalline phase as calcite, along with a variety of alumino-silicate peaks that align with minerals such as leucite and biotite, consistent with minerals found in other Pompeian mortars from early Imperial building phases (Supplementary Fig. 7)[33]. The similarity in all peak positions and relative peak intensities, and the degree of crystallinity across all samples, further demonstrated their compositional consistency.

Under plane-polarized light (PPL) and cross-polarized light (CPL) analysis, all of the samples (PM, MR, W1, W2, and W3) showed strong petrographic similarities (Supplementary Fig. 8). All samples contained primarily rounded, aphyric to poorly porphyritic volcanic aggregate composed of pumices and lithics. When combined with the findings from Raman (see below) and XRD, these results confirmed the presence of leucite, sanidine, and biotite in the lithics. The binders were predominantly microsparitic, with W1 showing some heterogeneity due to unmixed binder zones and calcite inclusions, and PM and MR exhibited homogeneous textures. Reaction rims were prominent between the unaltered volcanic glasses and binder in all samples, which are indicative of active pozzolanic/post-pozzolanic reactions. Lime clasts ranging from 0.2 to over 1 mm in size were also common, and exhibited porosity, birefringence, and shrinkage fractures (Supplementary Fig. 9).

SEM-EDS analysis on sample cross sections revealed porous lime clasts, with Si and Al relatively well distributed throughout the adjacent matrix. Ternary diagrams of Ca, Al, and Si ratios were generated[42] for all samples (Fig. 2), highlighting a distinct difference between W2 and the other samples, with PM and W1 displaying highly similar distributions and volume fractions of Ca, Al, and Si. The Ca/Si fractions within the PM and W1 matrix were slightly lower than in MR and significantly lower than in W2. The auto-correlation functions applied to the EDS maps further support this differentiation, with volume fractions for Ca, Al, and Si closely matching between PM and W1, while W2 showed notable divergence (see Supplementary Text). Additionally, the shapes of the autocorrelation and two-point cluster functions for PM, MR, and W1 were similar to each other, but distinct from W2, and markedly different from those observed in an ordinary Portland cement reference mortar (see Supplementary Text). The strong similarity between PM and W1 suggests a common origin, supporting the hypothesis that the dry, pre-mixed materials served as a source material for both mortar repairs and the construction of new Roman concrete wall sections.

SEM/EDS imaging and ternary diagram analyses of the lime clasts in samples PM and W1 (Fig. 3) showed that they are predominantly calcium-rich, and their corresponding Raman spectra (Fig. 3) revealed that they are primarily composed of calcite. These clasts are all characterized by distinctive cracking and a high degree of internal porosity, with some displaying signs of hollowing or partial dissolution (Fig. 3 sample MR). Elemental mapping also revealed increased concentrations of Al and Si, both around aggregates and along the rims of the lime clasts (Fig. 3, samples W1 and MR).

The lime clast crystallization kinetics were further investigated using transmission FTIR and mass spectrometry (Fig. 4, Supplementary Fig. 6). Using the same metrics as in Chu et al.[43], the v_2 and v_4 vibrational modes in the samples, located at approximately 870 cm^{-1} and 713 cm^{-1}, respectively, were analyzed after different durations of mechanical grinding in order to identify the extent of crystallinity of the carbonate phases. The v_2 and v_4 normalized values were plotted (see Fig. 4 (left)) for both the modern quicklime (mQL) and slaked lime (mSL) references, and the ancient (PM, W1, W3, IX10S-20, and IX10S-26) samples. A notable difference in the grinding curve slope was exhibited between the mQL and mSL samples, which was subsequently used as a reference to group the archeological samples into quicklime (red box) or slaked lime (blue box) precursors (Fig. 4 (left)). Since the

https://doi.org/10.1038/s41467-025-66634-7

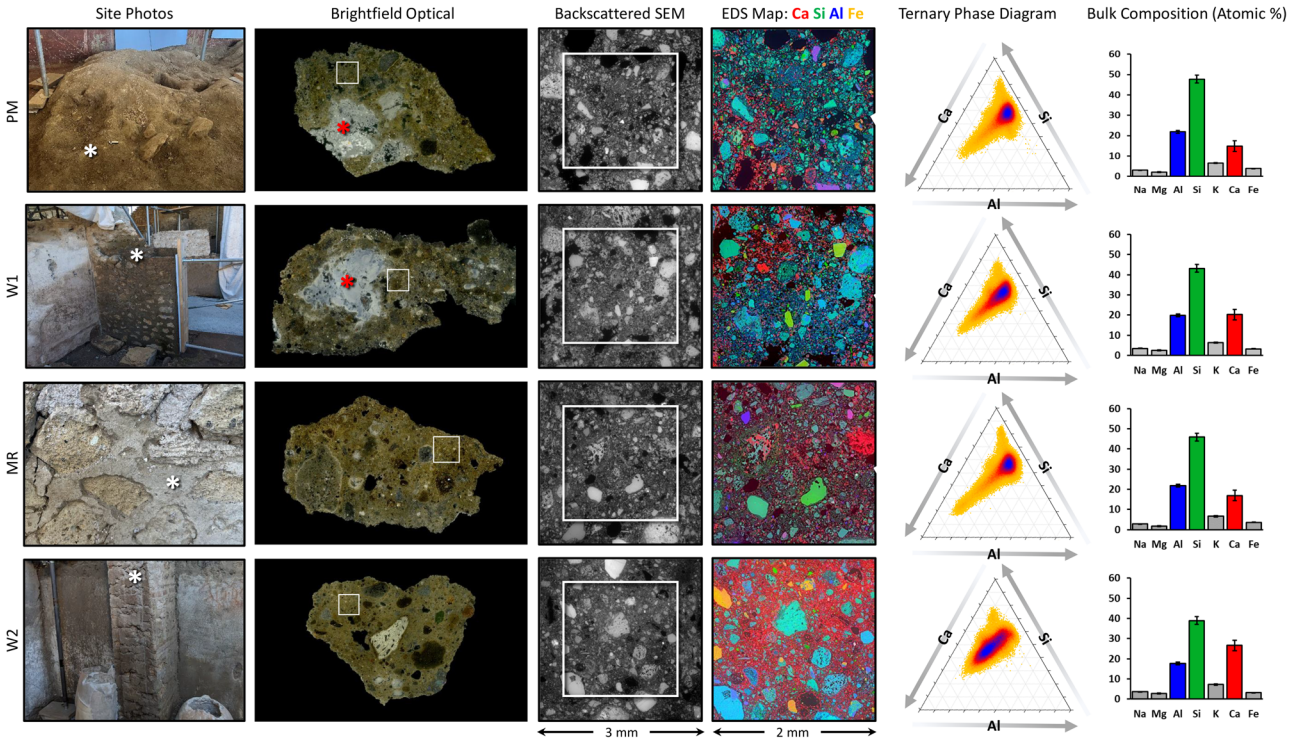

Fig. 2 | Microscopic and compositional analysis of the pre-mixed (PM) dry materials pile, pozzolanic mortars in two unfinished wall structures (W1 and W2), and the mortar utilized for wall repairs (MR). The leftmost column displays the locations of concrete samples from Roman architectural components (with points of sample collection denoted by white asterisks). The second column displays brightfield optical micrographs of cross sections of the pozzolan/lime pre-mixed dry materials and mortars, highlighting large lime clasts (denoted by red asterisks) in the PM and W1 samples, alongside a relatively uniform pozzolan-based matrix throughout all samples. The third and fourth columns present SEM backscattered electron micrographs and Energy Dispersive Spectroscopy (EDS) maps, highlighting the morphology and chemical composition of the pozzolan matrix. The ternary phase diagrams in the fifth column illustrate the compositional differences within the Ca-Al-Si system. The wall sample W2 clearly contrasts with other pozzolanic mortars and pre-mixed dry materials, all of which exhibit highly similar ternary diagrams. These results are corroborated by bulk composition quantification (atomic % of Na, Mg, Al, Si, K, Ca, and Fe) for each sample (column 6), showing a larger Ca concentration in W2 compared to other samples (average values plotted from $n = 3$, and error bars correspond to ± one standard deviation).

ν_2 and ν_4 vibrational modes are most sensitive to in- and out-of-plane lattice distortions, the shallower slope in the mSL and IX10S-20 samples suggests that $Ca(OH)_2$ underwent less extensive reconfiguration of its crystal structure over time (likely through hydration and carbonation), which would lead to the formation of more ordered phases which can be disrupted by an applied strain. In contrast, the steeper slope in the mQL sample implies a lower starting degree of order, and a more structurally uniform, but disordered material, where ν_4 changes minimally with progressive grinding. The alignment of the PM, W1, and W3 samples with the mQL reference line strongly supports the presence of carbonated quicklime as a raw material in these samples, which is suggestive of a rapid crystallization process. Across all samples, the unnormalized ν_2/ν_4 peak ratios were slightly lower than those reported in the literature for other archeological mortars, which could in part be explained by the presence of amorphous calcium carbonate in the lime, determined through TGA of the mQL and mSL reference samples (Supplementary Fig. 10).

Stable isotope mass spectrometry provides an additional method for investigating the environmental and chemical conditions that influenced the formation and alteration of ancient carbonate materials. This technique measures the ratios of the rare heavier isotopes to common lighter isotopes of carbon ($^{13}C/^{12}C$) and oxygen ($^{18}O/^{16}O$). Mass spectrometry can distinguish between different reaction environments because isotopic signatures vary depending on carbonation conditions, with shifts caused by differences in water availability and atmospheric CO_2 uptake during carbonation processes. For example, lime carbonation proceeding slowly in water-rich environments at near equilibrium conditions has a different signature than carbonation resulting from the rapid absorption of atmospheric CO_2 through a thin film of water, which can drive kinetic isotope fractionation. Equilibrium precipitation would have values near the origin, depending on local water composition, whereas the combined kinetic isotope effects from hydration of atmospheric CO_2, which follows a slope of ~0.6–0.7 in a $\delta^{13}C$ vs. $\delta^{18}O$ plot, and hydroxylation of atmospheric CO_2, which follows a slope of ~1, have a maximum negative $\delta^{13}C$ shift of 26–31‰ and $\delta^{18}O$ of 27–30‰. The relative importance of each kinetic process is pH dependent; in hot mixing, which occurs at high pH in water-limited conditions, hydroxylation is likely to be a dominant process[44] providing an independent method to differentiate between carbonation conditions (Fig. 4B).

Previous measurements of $\delta^{13}C$ and $\delta^{18}O$ by Kosednar-Legenstein et al.[45] of ancient Roman, Gothic, and Renaissance mortars and plasters show a broad scattering with a positive correlation between $\delta^{13}C$ and $\delta^{18}O$, with a slope of ~0.7 (Fig. 4B, gray symbols). The samples from the Pompeii archeological site overlap with these previously published values, but largely fall into two distinct populations (Fig. 4B). These populations correspond to materials identified as quicklime (red box) and slaked lime (blue box). mQL (the modern quicklime reference) is one end-member with the lightest $\delta^{13}C$ and $\delta^{18}O$ values. Within the ancient quicklime population, the light $\delta^{13}C$ and $\delta^{18}O$ values are consistent with large kinetic isotope effects from atmospheric CO_2 hydration and hydroxylation in a water-limited environment (Fig. 4B, red box). This pattern is consistent with hot mixing involving direct quicklime addition and in situ carbonation. Both the $\delta^{13}C$ and $\delta^{18}O$ values are heavier in the slaked lime samples from Pompeii, with IX10S-20 representing a second end-member (Fig. 4B, blue circles). These

https://doi.org/10.1038/s41467-025-66634-7

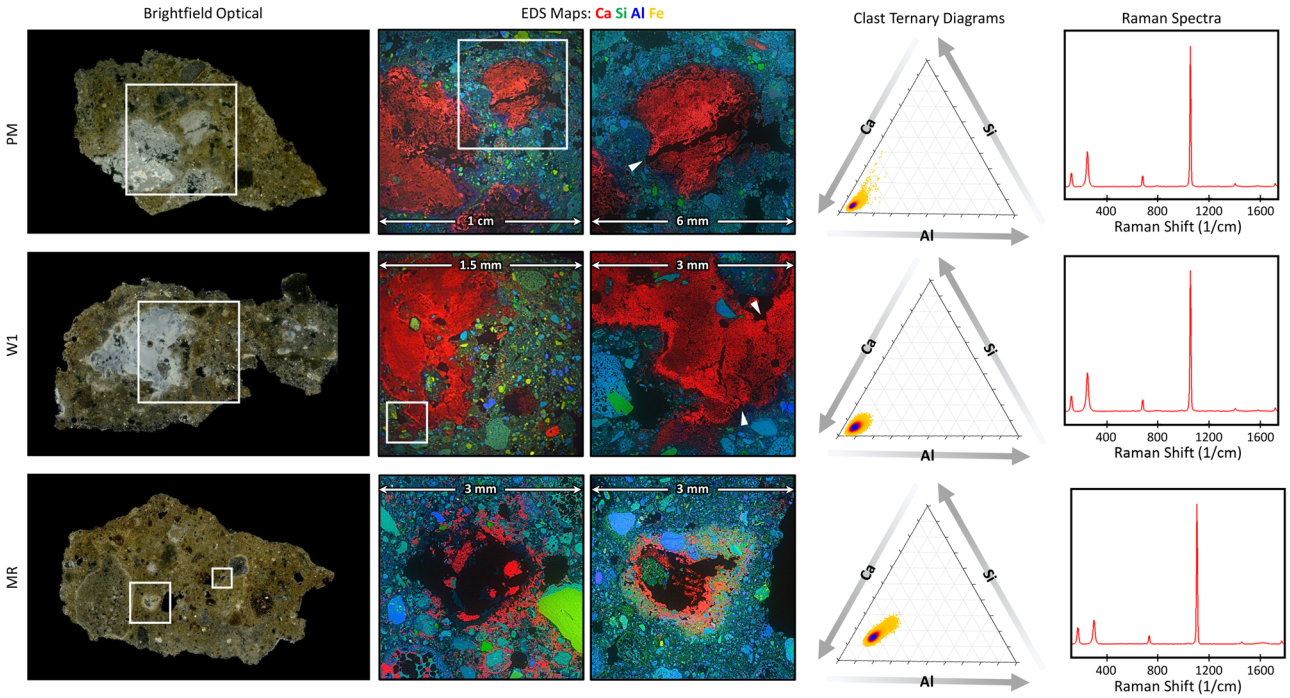

Fig. 3 | Microstructural and compositional analysis of lime clasts in the pre-mixed (PM) dry material pile, pozzolanic mortars in an unfinished wall (W1), and the mortar utilized for wall repairs (MR). Energy Dispersive Spectroscopy (EDS) maps show the elemental distributions of Ca, Si, and Al, with lime clasts appearing prominently in red, demonstrating their high calcium content. The top two rows (PM and W1) reveal lime clasts with similar characteristics, notably displaying distinctive cracking patterns (right EDS maps; cracks denoted with white arrowheads), which are indicative of the use of quicklime and hot mixing techniques. In contrast, the third row (MR) shows lime clasts undergoing evident dissolution, suggesting ongoing reactivity within the matrix that may contribute to long-term structural resilience through the progressive transformation of lime phases. The two rightmost columns provide ternary phase diagrams and Raman spectra of the clasts, showing their mineralogical composition and chemical environment within the matrix.

values suggest precipitation closer to isotopic equilibrium, with the $\delta^{13}C$ reflecting dissolved inorganic carbon and $\delta^{18}O$ reflecting precipitation from local water at ambient conditions. Importantly, all samples in this study were collected prior to modern restoration efforts, so the isotopic variations reflect the original construction practices rather than post-depositional interventions.

Post-pozzolanic aggregate/matrix interfacial remodeling

Across PM, MR, W1, W2, and W3, reaction rims were observed; Fig. 5 illustrates the reaction rims present around pumice particles in the mortar, offering details about the long-term chemical processes within the volcanic aggregate-matrix interfacial zones. The brightfield optical micrograph on the left indicates regions of interest within pumice particles situated in the cementitious matrix. These regions (highlighted by white boxes) represent areas where extended remodeling reactions are distinctly observable as reaction rims at the pumice-matrix interface. The EDS maps in the second and third columns show the elemental distributions within the interfacial zones, where two distinct features are observed: (i) calcium-rich mineralization (red) at the border and in the vesicles of the vitreous pumice aggregates, and (ii) Si and Al-rich mineralization (blue and green) in the vesicles of the pumice. The presence of these pumice fragments within these samples thus provides a unique opportunity to unequivocally identify these sites of chemical transformation, since new mineral formation can be clearly visualized within the native internal voids of the pumice fragments (Fig. 5).

The ternary phase diagrams and bar graphs reveal the compositional relationships of Ca, Si, and Al within the reaction rims (Fig. 5, right). Red regions denote the presence of Ca-rich phases with the elemental composition resembling Ca:Si:Al ratios of ca. 5:3:2, whereas the blue regions denote the presence of aluminosilicate phases with Ca:Si:Al ratios of ca. 1.5:6:2.5, and similar to the unaltered pumiceous glass. For a more comprehensive analysis of the various phases and their compositional differences, see Supplementary Fig. 11.

While these EDS mapping data can provide critical information regarding the elemental distributions within the different samples, they cannot identify the specific mineral polymorphs present. Raman confocal imaging enables the spatially resolved identification of mineral phases within pore spaces, revealing post-depositional transformations in the pumice glass matrix. This technique can be employed to help trace mineral evolution in the vesicles, offering a clearer understanding of in situ chemical and environmental changes (Fig. 6). The Raman spectra demonstrate calcite (the most stable polymorph of $CaCO_3$) as the dominant mineral phase, which exhibits characteristic Raman peaks including the symmetric stretching mode of carbonate groups (~1085 cm^{-1}) and lattice vibrational modes at ~280 cm^{-1} and ~155 cm^{-1}. In addition to calcite, the Raman data also revealed the presence of aragonite (a less stable polymorph of $CaCO_3$), identified through its distinct peaks, including the symmetric carbonate stretch at ~1085 cm^{-1} (shared with calcite), v_4 doublet at 701 and 706 cm^{-1}, and characteristic lattice modes at ~208 cm^{-1} and ~152 cm^{-1}. The simultaneous presence of calcite and aragonite in the vesicles of the pumice glass suggests that post-pozzolanic carbonation processes have been influenced by localized variations in chemical conditions, such as Mg/Ca ratio, temperature, and kinetics during the carbonation stage[22]. The dissolution and recrystallization of carbonates into stable calcite and aragonite forms a self-repairing layer at the interface (Fig. 6, Raman maps). Interestingly, the Raman data do not show significant peaks associated with aluminosilicate frameworks, demonstrating that previously literature-reported[46] crystalline zeolites, such as chabazite ($K_2CaAl_4Si_8O_{24}{\cdot}12H_2O$), are absent or poorly represented in the vesicles of the pumice glass. However, the detection of significant levels of Si and Al in the SEM-EDS data suggests the presence of an amorphous or poorly crystalline aluminosilicate matrix (most likely C-A-S-H),

https://doi.org/10.1038/s41467-025-66634-7

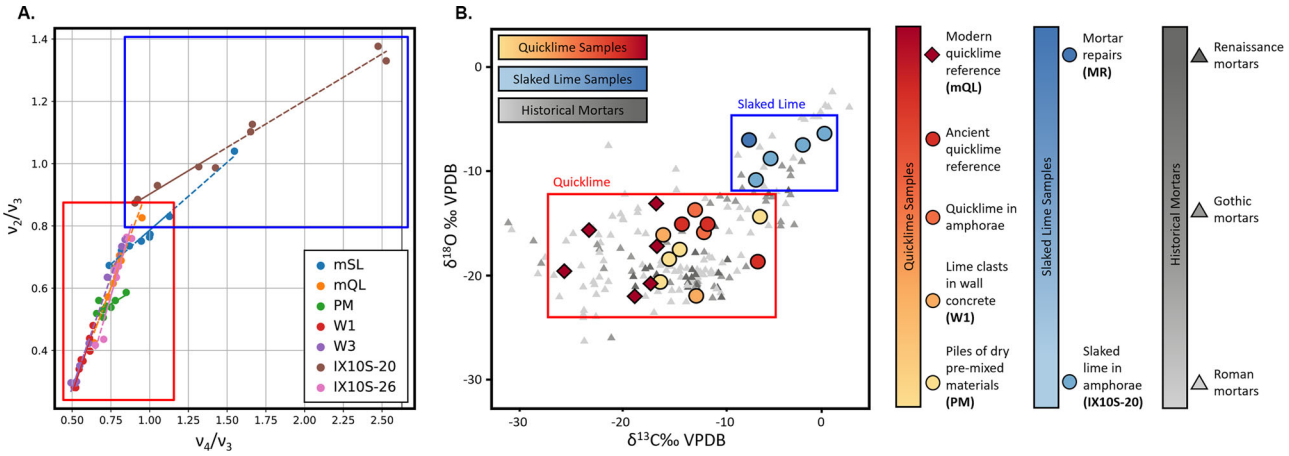

Fig. 4 | FTIR and isotopic analyses differentiate quicklime and slaked lime in ancient samples. A Normalized transmission FTIR vibrational mode intensity ratios across samples from this work, subjected to progressively longer grinding times. The distinct slopes of the modern reference slaked lime and quicklime (mSL and mQL) grinding curves were compared to the lime in the ancient samples. The lowest v_2/v_4 ratios were observed for samples identified as ancient quicklime (grouped in red the red box), suggesting a lack of long-range initial order. The grouping in the blue box shows samples with higher v_2/v_4 ratios, suggesting the presence of slaked lime. **B** $\delta^{13}C$ and $\delta^{18}O$ isotopic compositions of carbonate samples from Pompeii (circles), modern samples (diamonds), and ancient Roman, Gothic, and Renaissance mortars and plasters from Kosednar-Legenstein et al. (gray triangles). Samples with quicklime clasts from Pompeii (red and orange circles) are lighter in both $\delta^{13}C$ and $\delta^{18}O$ (grouped in the red box) than the Pompeii-collected slaked lime samples (blue circles), and approach values from modern quicklime (mQL, dark red).

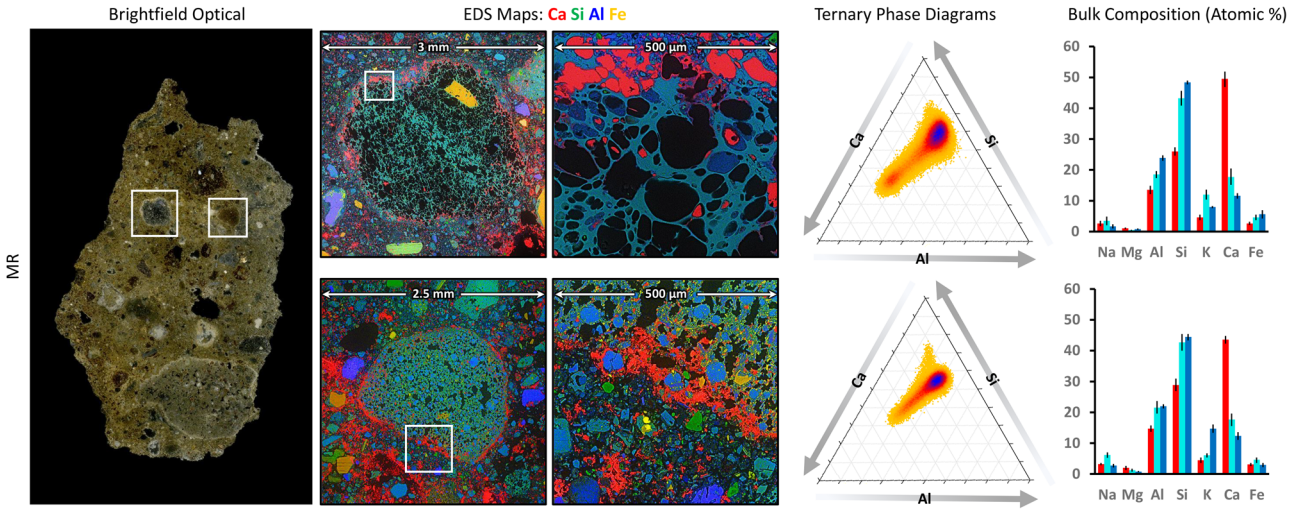

Fig. 5 | Remodeling at the volcanic aggregate/cement matrix interface in the MR sample. Brightfield optical micrograph (left) displays the cross-sectional view of the sample with distinct volcanic aggregates embedded in the cement matrix (denoted by the white boxes). EDS elemental maps (second column) of two entire volcanic aggregates reveal elemental distributions, emphasizing the complex interplay between Ca, Si, and Al across the pumice/cement boundary, and a clearly visible enrichment in calcium at the interface. Ternary phase diagrams of the interfaces (fourth column) demonstrate compositional trends reflecting interfacial remodeling, with two main regions in the diagram: one (upper) more intense, containing less calcium and more Si and Al; and one (lower) more enriched in calcium. The compositions of red, blue, and cyan regions are plotted using compositional histograms (fourth column), showing the atomic percentages of Na, Mg, Al, Si, K, Ca, and Fe. These results show localized chemical variability of mineral remodeling, implying two main phases at the interface: (i) a blue phase rich in Si, Al, and some Ca, and (ii) a red phase rich in calcium with some amount of Si and Al (average values plotted from $n = 3$, and error bars correspond to ± one standard deviation).

potentially originating from residual pozzolanic reaction products or volcanic glass. The precipitation of calcite, aragonite, and C-A-S-H not only stabilizes the concrete but also reduces porosity by filling microcracks and voids, hence improving resistance to water intrusion.

Discussion

The goal of this work was to provide insights into Roman building technologies and their practical applications, considering the rare opportunity to explore a well-preserved and active ancient construction site. The analysis of raw materials and Roman concrete in the context of Pompeii also has the potential to significantly influence the development of their modern material analogs, contributing to the development of restoration and repair mortars that are compatible with ancient materials and, at the same time, more durable and sustainable from an environmental perspective. The variety of materials, including pozzolana, limestone, tile fragments, common ceramics, amphorae, dry pre-mixed piles of lime, pozzolanic sand, and Neapolitan Yellow tuff, highlights the extensive nature of the work being undertaken at the site. The careful storage and preparation of these materials suggest that significant reconstruction and restoration efforts were underway at the time of the eruption, aimed at repairing and enhancing the structural integrity of the dwelling. The presence of

https://doi.org/10.1038/s41467-025-66634-7

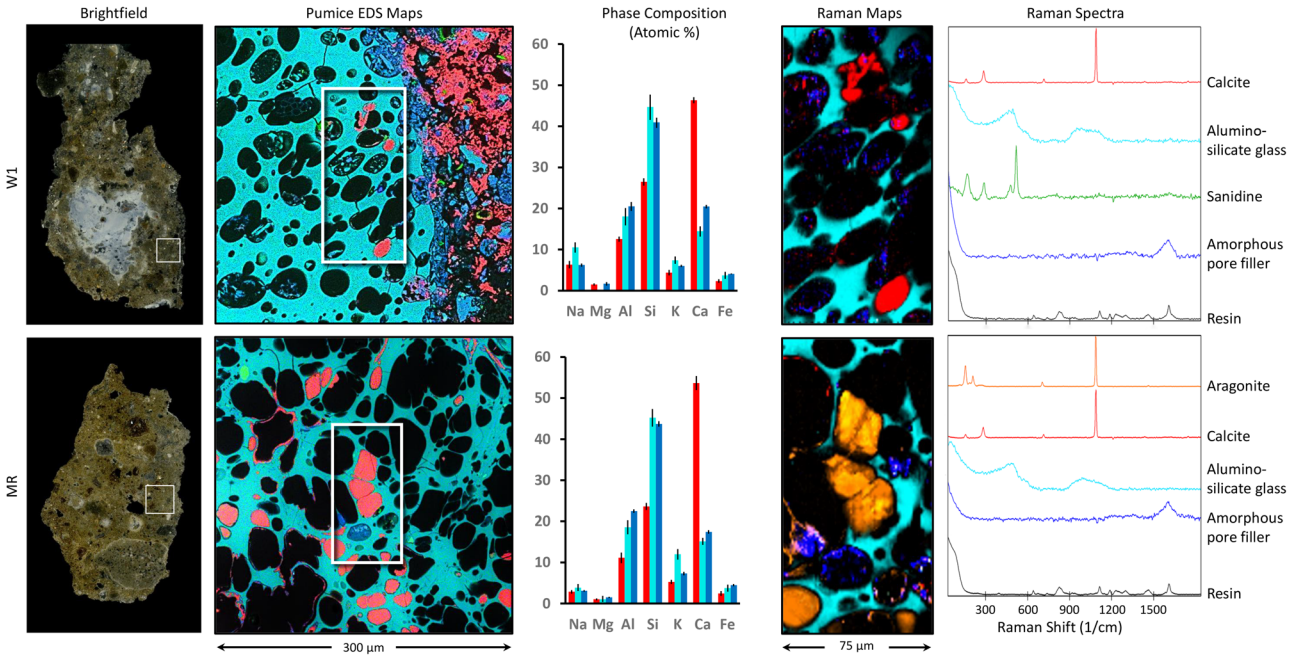

Fig. 6 | Comparative microstructural and compositional analysis of the W1 and MR samples. Brightfield optical micrographs from the sample cross-section (left) show macroscopic features, including large lime clasts and a pozzolanic matrix (W1). Pumice EDS maps (second column) highlight elemental distributions at the pumice/cement matrix interface. The phase composition histograms (third column) plot atomic percentages of Na, Mg, Al, Si, K, Ca, and Fe in the red, blue, and cyan regions (average values plotted from $n = 3$, and error bars correspond to ± one standard deviation). Raman maps (fourth column) reveal chemical variations in the inclusions, with characteristic spectra (right) identifying phases such as calcite, alumino-silicate glass, sandine, amorphous pore fillers (in W1), and aragonite (in MR).

dismantled roofing tiles and the systematic organization of materials further underscore the comprehensive and ongoing nature of the construction activities in the *domus*.

The materials were also sorted and stored in different rooms according to type and purpose. For example, the *atrium* likely served as a central hub for pre-mixed dry lime and pozzolanic sand, essential for mortar preparation, while room 28 was primarily used for storing tiles and stonework. Additionally, the fountain pool in room 2 and the surrounding area were likely used for adding water to the dry materials during mixing. This systematic approach would have allowed workers to efficiently access and utilize materials as needed during the reconstruction process, minimizing delays and ensuring that the work progressed smoothly.

The pronounced resemblance between the PM and W1 samples suggests a shared origin, bolstering the hypothesis that dry, pre-mixed materials functioned as the source material for new Roman concrete wall segments. Although the overall bulk compositions are similar, the elevated calcium:silicon (Ca/Si) ratios observed in the MR and W2 matrices, as compared to PM and W1, suggests the possible inclusion of additional Ca-rich material during their preparation. Based on the available evidence, slaked lime might have been deliberately added to some of the previously hot-mixed base mixtures. This practice could have been employed to enhance the workability and specific structural properties of the finishing mortars, optimizing them for repair and construction applications. The compositional tuning observed in MR and W2 highlights an adaptive approach in Roman mortar production, where material adjustments were potentially employed to meet distinct functional demands, ensuring optimal performance in various construction contexts. In support of this interpretation are the lime-containing amphorae found in corridor 10 and courtyard 12 (Supplementary Fig. 5). In addition to preparing repair mortars (MR), slaked lime from the amphorae was most likely used to apply the *arriccio* and *intonachino* layers of the pictorial coating that was being deployed inside the *atrium* and room 8.

The uniformity in aggregate composition, reaction rims, and lime clast characteristics observed in petrographic analyses across the PM, MR, W1, W2, and W3 samples suggests a shared material source (likely from the surrounding Somma-Vesuvius region) and consistent preparation methods. The similarity in mineralogy and structure between PM and W3 is particularly notable, as it demonstrates that material from this pre-mixed raw material pile was not only consistent with actively repaired or built features (as in MR and W1), but was also employed in the production of structural masonry. The widespread presence of coarse, birefringent lime clasts with high internal porosity and internal cracking that are characteristic of incomplete hydration supports our proposed usage of hot mixing across sample contexts.

The results from the present study suggest the common use of hot-mixing techniques for several different applications at the investigated excavation site. While for larger-scale imperial constructions, the logistics of conducting batch hot mixing may have posed challenges, evidence from large-scale sites like Augusta Raurica suggests that hot mixing was still effectively employed, supported by extensive on-site mixing platforms and prearranged material staging areas[31]. The morphology and presence of lime clasts in the analyzed mortar and raw material piles support the usage of quicklime through several avenues of evidence. Firstly, observing lime clasts in mortar is a key indicator of hot mixing, as lime clasts persist through the prevention of lime dissolution, which is driven by the exothermic hydration reaction of quicklime during mixing[2,15]. Additionally, the cracking and expansion characteristics are typical of the mortar hydration process with quicklime, where quicklime expands and cracks upon reacting with water in the mortar mix. This process is distinct from the morphology of relict lime inclusions within poorly mixed slaked lime, which would instead exhibit a more homogeneous distribution, and without pronounced expansion and cracking[20].

The relatively low FTIR v_2/v_4 peak ratios in the samples, particularly the prominence of the v_4 peak, suggest a distinct formation environment in the lime clasts compared to previously studied

archeological mortars, where the calcite was taken from the mortar matrix. A higher v_4 intensity relative to v_2 could suggest a carbonate-dominated composition associated with a prolonged, controlled carbonation process. This ratio profile is consistent with a hot mixing approach where quicklime reacts in a low-moisture environment, preserving Ca-rich amorphous phases within lime clasts that later carbonate in situ over time (the presence of amorphous phases has been confirmed through thermogravimetric analysis (Supplementary Fig. 8). The similarity between PM, W1, W3, and IX10S-26 and the mQL samples supports the notion that the ancient samples formed through a hot-mixed process with a controlled, gradual carbonation environment that stabilizes the microstructure.

The two-point cluster function applied to EDS maps of the ancient mortar samples shows a higher initial value at smaller distances compared to a modern reference cement paste (OPC). These results suggest that the phases in the ancient samples are more closely packed, suggesting a denser and more interconnected microstructure. Such a structure is characteristic of materials where the phases are allowed to grow and connect without significant interruption, which is indicative of a consistent and simultaneous hydration process. The ancient samples also exhibit a near-horizontal trend at longer distances in the cluster function, implying that the clustering does not significantly decrease with distance. This continuity suggests a uniform distribution of phases, which again is consistent with the hot mixing process where quicklime and pozzolans are mixed dry and then hydrated together, ensuring a thorough and consistent mixing, and leading to a uniform microstructure with well-distributed phases. In contrast, the OPC reference sample shows a more pronounced drop-off in the two-point cluster function, demonstrating a less connected microstructure with more isolated clusters of elements (see Supplementary Text).

Carbon and oxygen isotopic analysis of the different material samples substantiates the hypothesis that both quicklime and slaked lime were utilized in the formulation of Roman concretes. The materials from the Pompeii construction site have $\delta^{18}O$ values consistent with large kinetic isotope effects, along with a range of intermediate $\delta^{13}C$ values reflective of variably expressed kinetic fractionation. The mQL sample has lighter $\delta^{13}C$ values compared to the Pompeii construction materials and most of the ancient materials from Kosednar-Legenstein et al.[45]. This observation may be attributable to the Suess Effect, whereby post-industrial atmospheric CO_2 is ~2‰ lighter in $\delta^{13}C$ because of an additional contribution from fossil fuel combustion[47]. Some of the Pompeii samples, including PM and W1, have similarly light $\delta^{18}O$, suggesting similar kinetic isotope effects were at play (Fig. 4, warm-colored circles). In samples IX10S-20 and MR, the isotopic signature is closer to expected equilibrium and likely reflects the presence of abundant water, slower carbonation, and equilibrium fractionation with dissolved inorganic carbon and the isotopic composition of the local water used in slaking[45,48]. The distinct isotopic compositions substantiate the hypothesis that both quicklime and slaked lime were utilized in the formulation of Roman mortars, and could thus be employed as a valuable tool for future diagnostic purposes. These findings support the use of hot mixing as a primary method for preparing Roman architectural mortars and the use of slaked lime to repair and finish mortars (e.g., MR), to improve their workability.

The presence of Ca-rich rims around aggregates, the dissolution of lime clasts, and the formation of $CaCO_3$/C-A-S-H composite layers around volcanic pumiceous glass aggregates provide critical further evidence of our previously proposed self-healing mechanism for these materials. Firstly, the hollowing observed in some clasts is indicative of their long-term dissolution and their critical role as reactive Ca sources within the matrix. The post-pozzolanic stages of the mortar's lifecycle correspond to processes that occur after most of the free lime ($Ca(OH)_2$) is consumed through pozzolanic reactions or carbonated with atmospheric CO_2 to form calcite-rich lime clasts (it is known that hot mixing favors lime clasts formation). The atmospheric CO_2 in the pore solution lowers the pH, which leads to the dissolution of the lime casts, releasing Ca-rich fluids into the surrounding pore network. The dissolved carbonate and bicarbonate species from carbonated pore fluids rich in Ca ions then contribute to additional calcium carbonate precipitation (Eq. (2), Eq. (3)).

$$Ca^{2+} + CO_3^{2-} \rightarrow CaCO_3 \tag{2}$$

$$Ca^{2+} + HCO_{3^-} \rightarrow CaCO_3 + H^+ \tag{3}$$

The EDS maps (Fig. 5) clearly show elevated Ca concentrations in both dissolved lime clasts and the volcanic aggregates/cement matrix interfaces, confirming the progressive redistribution of calcium. At the pumice/matrix interface, carbonated pore fluids rich in dissolved calcium react with the surfaces of volcanic glass, promoting the precipitation of carbonate minerals such as calcite and aragonite within pores and voids. Although aragonite is metastable under ambient conditions and may later transform into calcite, its persistence in Roman concrete suggests a protective microenvironment within voids or vesicles, where it remains stable due to the unique chemistry of the system. The formation of aragonite alongside calcite highlights the dynamic geochemical evolution of the concrete, where both polymorphs contribute to the reduction of porosity through pore filling, matrix densification, and stabilization of the microstructure. Elemental mapping shows that the mineralized matrix also contains significant quantities of Si and Al. These elements are likely present as amorphous phases, such as C-A-S-H or partially altered volcanic glass, which lack the long-range order necessary to produce detectable Raman peaks. The absence of Raman signals for Al-tobermorite and stratlingite, or zeolitic phases like chabazite ($K_2CaAl_4Si_8O_{24}{\cdot}12H_2O$) or phillipsite ($KCaAl_3Si_5O_{16}{\cdot}6H_2O$) in the Ca-rich void fillings suggests that these phases, if present at all, are in very low quantities. The possibility of crystalline analogs of C-A-S-H cannot be ruled out due to fluorescence interference in Raman spectra associated with the elevated Fe content in some regions of the aggregate/matrix interfacial zone[22,46]. The amorphous, Ca- and Al-rich phases are likely the result of in situ precipitation rather than inherited volcanic calcite inclusions, as evidenced by the lack of crystalline characteristics typical of volcanic minerals, and the presence of zoned, reaction interfaces around the pumice fragments, which is incompatible with inherited detrital grains[49].

The above-described post-pozzolanic remodeling not only consolidates but also improves concrete's mechanical properties over time, giving rise to crack propagation resistance and enhanced durability. The composite matrix of vesicle- and pore-filling phases of calcite, aragonite, and C-A-S-H underscores the complex crystallization processes at play. This interplay of carbonation and pozzolanic activity at the aggregate/matrix interfacial zone effectively acts as a self-healing mechanism within the concrete. Over centuries, these chemical processes continuously reinforce the concrete by forming stable mineral phases at the interface, which fill in voids, reduce permeability, and help maintain structural integrity.

The findings from the excavation and analysis of *Domus* 1 in block 10 of Regio IX in Pompeii provide compelling insights into the advanced construction techniques employed during the final phase of the city's restoration efforts prior to the eruption of Mount Vesuvius in 79 CE. The comprehensive examination of materials, including mortar samples and construction tools, reveals a systematic and highly organized approach to building, characterized by the careful preparation and storage of raw materials (see Fig. 7). This organizational framework likely facilitated efficient construction processes, allowing for the repair and enhancement of structural elements.

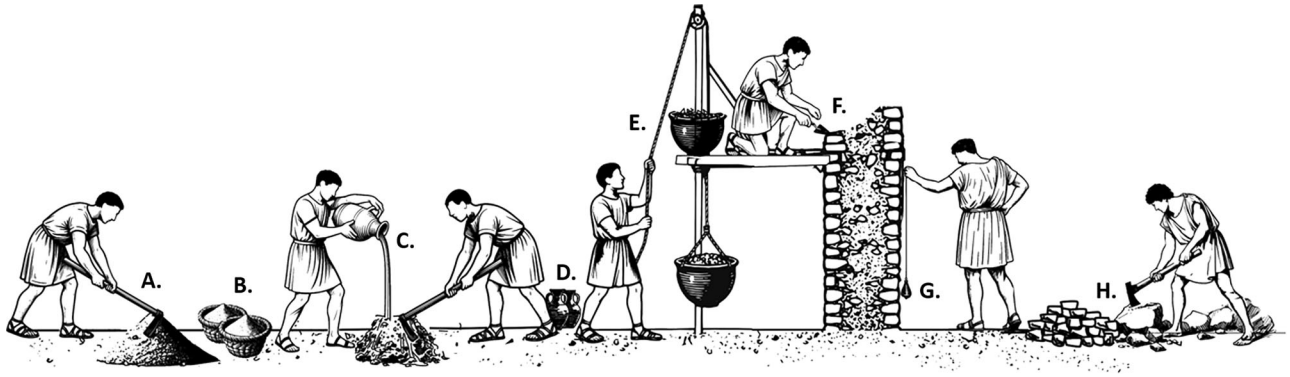

Fig. 7 | Schematic summary of the ancient production of Roman concrete. Each step in the schematic captures a specific part of the preparation and building process, highlighting both the materials and the tools used. **A** Preparing the dry mortar mix: This process begins with a dry, pre-mixed pile of pozzolan and quicklime. **B** Adding *cocciopesto*: To enhance the mortar's water resistance and durability, Romans often added *cocciopesto*, a mix containing ground terracotta or pottery fragments. **C** Hydrating the mortar: The dry mortar mixture is then hydrated, where workers would carefully add water to initiate a chemical reaction with the quicklime. **D** Slaking lime: slaking, or hydration of quicklime to produce slaked lime before being added to the mortar mix, often took place in smaller vessels. This step was not included in the preparation of Roman concrete and was generally used in the preparation of finishing and repairing mortars and fresco decorations. **E** Transporting mortar in broken amphorae: Broken amphorae, or pottery vessels, served as practical containers for moving mortar. These vessels were readily available on Roman construction sites and were a sustainable choice, repurposing broken pottery that would otherwise be discarded. **F** Applying the mortar with a trowel: The mortar was then moved to the wall and applied with a trowel, carefully layering it between *caementa* and stones or bricks. **G** Ensuring geometric and structural integrity with a plumb line: As construction progressed, workers used a plumb line to verify vertical alignment. This simple yet effective tool helped maintain precision during the construction process, which was essential for stability, especially in tall or expansive structures. **H** Shaping aggregate with an ax: To create aggregate, an essential component of Roman concrete, workers used axs to break larger stones into smaller pieces.

This study significantly advances our understanding of Roman construction technology by providing multiple lines of evidence for the use of quicklime in a hot mixing process, a method that appears to contradict the traditionally accepted interpretations of Vitruvius' writings. The presence of lime clasts within the mortar, alongside the distinctive microstructural characteristics identified through advanced imaging techniques, strongly supports the hypothesis that quicklime was mixed directly with pozzolanic materials and water, generating the high temperatures necessary for the rapid setting and enhanced durability of the mortar. Moreover, the microstructural analysis, including the application of autocorrelation and two-point cluster functions, demonstrates a high degree of uniformity in the construction materials used across different areas of the site. This consistency suggests that pre-mixed dry materials were a central component of the construction strategy, providing a ready source of high-quality mortar that could be used efficiently in both new construction and repair work. This evidence further demonstrates that these pre-mixed dry materials were likely prepared using quicklime, which played a critical role in achieving the desired structural properties of Roman concrete.

Utilizing FTIR and isotope analysis for comparing the pre-carbonation history of lime in mortar suggests a promising avenue for distinguishing these production methods, given the differing kinetics at play in the preparation of quicklime and slaked lime. The data presented here support the addition of quicklime directly into the mortar and use in the dry, pre-mixed material pile, and provide insights into lime clast dissolution and remineralization, driven by the combined effects of ongoing pozzolanic reactions and weathering cycles leading to the release of reactive Ca ions. The deposition of recrystallized phases, including calcite, aragonite, and amorphous phases at aggregate interfaces and within vesicles, reveals a level of chemical complexity and post-pozzolanic reactivity previously uncharacterized in ancient construction materials.

The implications of these findings extend beyond just archeological inquiry, offering valuable insights for modern conservation efforts. By understanding the specific methods and materials used in ancient Roman construction, contemporary restoration practices can be more accurately tailored to match the original techniques, ensuring that repairs are both historically authentic and structurally sound. This research underscores the importance of integrating scientific analysis with historical and archeological perspectives to reconstruct ancient technologies and apply them to the preservation of cultural heritage.

While the results reported in the present study provide clear evidence for the use of hot mixing in both the original construction (W3) of *Domus IX 10, 1* as well as repairs performed after the major earthquake in 62 CE (W1, MR, and MP), these discoveries are of much broader significance from a methodological and historical perspective. While previous studies could only speculate on the precise methods of Roman mortar and concrete production, our combination of archeological evidence, combined with petrographic, EDS, Raman, X-ray diffraction, and isotopic approaches, have been employed to confidently distinguish between the use of quicklime and slaked lime in the synthesis of these materials, providing a robust path forward to assess the broader spatial and temporal application of each approach across the Roman Empire.

Methods

All archeological sampling and analytical work were conducted under the 51956544MIT_ITALY (PA-POMPEI, 15/12/2023, CONVENZIONI ITALIA 62) agreement between the Parco Archeologico di Pompei and Massachusetts Institute of Technology, in full compliance with all required permits, local regulations, and best practices, ensuring provenance, transparency, and adherence to heritage protection laws. Field sampling in Regio IX, Pompeii, took place between January 2024 and May 2025 under the supervision of park and conservation authorities. All archeological samples are permanently curated under the authority of the Parco Archeologico di Pompei, Italy.

Embedded and polished thin sections of collected centimeter-sized samples from each location were prepared by a commercial third-party vendor. To prepare reference samples of quicklime and slaked lime, laboratory-grade calcium carbonate was first calcined at 850 °C for 24 h. The calcined material was allowed to naturally carbonate for two years in ambient, dry conditions and was used as the modern quicklime (mQL) reference. To produce the modern slaked lime (mSL) reference, the freshly produced quicklime was hydrated and mixed using a 1:7 lime:water ratio. The resulting materials were

allowed to dry and carbonate under ambient conditions for two months. To verify the content of the lab-made control samples, small quantities of each were ground with an agate mortar and pestle for 30 s and subsequently analyzed using a Nicolet iS5 FTIR spectrometer (ThermoScientific, Madison, WI) in Attenuated Total Reflectance (ATR) mode across a wavenumber range of 4000 to 400 cm^{-1}, with a resolution of 4 cm^{-1}. The spectra were then processed with the OMNIC software package (Madison, WI) in order to perform baseline correction, background noise subtraction, and improve peak resolution. Analysis of absorption peaks and their corresponding wavenumbers was compared to reference IR spectra from the RRUFF™ database (Berlin, Germany), enabling the qualitative determination and confirmation of the samples' chemical compositions. To specifically investigate the kinetics of lime clast formation, the spectrometer was used in transmission mode on drilled quantities containing only the clast material, which were powdered with an agate mortar and pestle. Analysis was performed per the "grinding curve" methodology developed by Chu et al., with grinding times up to 15 min[43]. This method utilizes progressively longer durations of mechanical grinding with an agate mortar and pestle (from 0–15 min) to induce different levels of lattice strain and atomic disorder, and analyzes changes in the resulting IR vibrational mode peak intensities to provide insights into the kinetics of formation and degree of short-range order of different carbonate materials[43]. The peak intensities of the diagnostic carbonate IR vibrational modes (ν_3 (1420 cm^{-1}, asymmetric CO_3 stretching mode), ν_2 (874 cm^{-1}, out of plane CO_3 bending mode), and ν_4 (713 cm^{-1}, in plane CO_3 bending mode)) are then plotted as ratios (the "grinding curves"), normalized by the most IR-active vibration mode (ν_2/ν_3 and ν_4/ν_3). By measuring the slopes of these grinding curves, it is possible to systematically differentiate geogenic, synthetic, and pyrogenic carbonates, evaluate material disorder, and assess structural strain in lime-based materials.

To determine the crystallinity and mineral composition of these powdered Pompeii-collected samples, a Panalytical (Malvern, UK) Aeris Research diffractometer, using copper Kα radiation in a Bragg-Brentano geometry, was employed, spanning a 2θ range from 2° to 90°. The resulting diffraction patterns were analyzed using the HighScore Plus software package with the ICDD PDF-4 database.

Elemental analysis, used to complement the microstructural data, was conducted via semi-quantitative SEM-EDS, with elemental mapping employed to examine the composition and spatial distribution of the different mortar phases. Embedded and polished thin sections of each sample, prepared by a commercial third-party vendor, were imaged uncoated in low vacuum mode (15 Pa) at 20 keV using a Tescan (Brno, Czech Republic) Vega GMU scanning electron microscope equipped with a Bruker (Billerica, Massachusetts) XFlash 5030 dual-detector EDS system. The obtained EDS maps were further processed to generate matrices representing atomic percentages of elements such as Ca, Si, Mg, Al, and O, which were then visualized in ternary diagrams. The individual elemental maps for Ca, Si, and Al were further processed into an 8-bit form using ImageJ (NIH and LOCI, Madison, WI), and then run through a correlation function code in MatLab (MathWorks, Natick, MA)[50]. This approach provided information about the phase volume fractions and particle sizes of the Si, Al, and Ca-containing components in the samples, producing qualitative data for the generation of correlation and cluster functions (see Supplementary Text). The polished thin sections were further analyzed under plane-polarized light (PPL) and cross-polarized light (CPL) using a petrographic microscope to evaluate binder texture, aggregate composition, porosity, and lime clast morphology.

To investigate the distribution of the different material phases, correlative Raman spectroscopy was also performed on the same thin sections used for the SEM/EDS studies. A confocal Raman microscopy system (Alpha 300RA; WITec, Germany) was used to collect Raman spectra ranging from 0–3700 cm^{-1}. The system was equipped with an Nd:YAG 532 nm laser, a 600 g/mm grating UHTS Raman Spectrometer (WITec, Germany), and a CCD-camera cooled to −60 °C, and the excitation wavelength was calibrated by matching the T_{2g} mode peak of a Si wafer to 520 cm^{-1}. During the collection of the Raman mapping data, each spectrum was accumulated for 0.3 s with a lateral resolution of ca. 1 µm, and the resulting data were processed using the WITec Project 5 software package. After background removal, the signal from the embedding resin was subtracted from each scan, and maps plotting the relative abundance of each component were generated. For the single Raman spectra shown in Fig. 3a 10 s accumulation time was used.

To quantify the fractionation in carbon and oxygen isotope values, powder samples were collected with a small dental drill using a 0.5 mm carbide bit. Depending on the size of the specific phases of interest, 2–10 mg of powder were collected. Isotope analyses were performed on carbonate powders using a Nu Perspective Isotope ratio mass spectrometry system (Nu Instruments, Wrexham, UK). Samples were heated to remove water and volatiles before acidification in a NuCarb automated sample preparation unit held at 70 °C. Carbonate samples weighing 50–100 µg reacted for 25 min in individual glass vials with 150 µl orthophosphoric acid ($\rho = 1.93$ g/cm^3), and the evolved CO_2 gas was purified cryogenically. Purified sample gas and reference gas of known composition were alternately measured on six Faraday collectors (m/z 44–49) in 6 cycles, each with a 30-s integration time (3 min total integration time). Each session of approximately 50 individual analyses began with two ETH anchors, then alternated between blocks of six to eight unknowns and two ETH anchors, totaling eight anchors per run. Data were processed using the "D47crunch" Python package[51] with IUPAC 17 O parameters and 70 °C ^{18}O acid fractionation factors of 1.00871 for calcite[52]. Raw measurements were corrected using a pooled regression approach[51] using ETH anchor values from Bernasconi et al.[53]. Nominal anchor values for $\delta^{13}C$ and $\delta^{18}O$ are ('ETH-1': 2.02, −2.19; 'ETH-2': −10.17, −18.69; 'ETH-3': 1.71, −1.78, 'ETH-4': −10.2, −18.81, 'IAEA-C1': 2.42, −2.31; 'IAEA-C2': −8.25, −8.94; 'CIT': 2.05, −1.40). The ratios are reported as $\delta^{13}C$ and $\delta^{18}O$ in deviations from 0 in units of permil (‰) relative to the isotopic ratios in a standard material (i.e., Vienna Pee Dee Belemnite, VPDB).

Statistics and reproducibility

In total, six sections were examined from each sample, and the imaging, mapping, and spectroscopic results reported here are representative of the trends observed. For the bar graph data displayed in Figs. 2, 5, and 6, the solid bars denote the average values obtained from three different regions of interest, and the error bars correspond to +/- one standard deviation.

Reporting summary

Further information on research design is available in the Nature Portfolio Reporting Summary linked to this article.

Data availability

All data needed to evaluate the conclusions in the paper are present in the paper and/or the Supplementary Information. Supplementary Table S1 lists sample metadata (name, description, location, and modern/ancient designation). Supplementary Figs. S1–S5 document field context (site map, construction marks, tools, premixed materials, and amphorae with lime). Supplementary Figs. S6–S7 present FTIR (ATR and transmission) spectra and bulk powder XRD patterns. Supplementary Figs. S8–S9 provide petrographic micrographs of aggregates, binders, lime clasts, and marble-like grains. Supplementary Fig. S10 reports thermogravimetric analyses of modern slaked lime and quicklime. Supplementary Figs. S11–S13 include EDS elemental maps, compositional ternary plots, and imaging/elemental mapping for representative samples. Supplementary Fig. S14 illustrates correlation/cluster function concepts, and Supplementary Figs. S15–S16

show auto-correlation and two-point cluster function results. Supplementary Note S1 details the image-processing and spatial-statistics workflow, and Supplementary Note S2 provides petrographic thin-section descriptions for each sample. No public repository deposition of data is possible due to legal and ethical restrictions associated with the archeological context and cultural heritage protections governing the study area. These data include archeological material and sample information belonging to the Archeological Park of Pompeii, which are subject to national heritage laws and site-specific access regulations. Access to the data is restricted but can be requested by contacting Dr. Valeria Amoretti (valeria.amoretti@cultura.gov.it) and Dr. Antonino Russo (antonino.russo@cultura.gov.it). Requests will be evaluated by the Pompeii Archeological Sites according to their data sharing and permissions policy.

References

1. Lechtman, H., Hobbs, L. & Kingery, W. D. Roman concrete and the Roman architectural revolution. in *Ceramics and Civilization. Volume 3: High Technology Ceramics: Past, Present, Future*. **3**, 81–128 (American Ceramics Society, 1986).
2. Lancaster, L. C. *Concrete Vaulted Construction in Imperial Rome*. (Cambridge University Press, New York, 2005).
3. McCormick, M., Huang, G., Zambotti, G. & Lavash, J. Roman Road Network (version 2008). in *Digital Atlas of Roman and Medieval Civilization*. 2525620, 413570, 1307, 3276, 465, 68420, 1531156, 57332 Harvard Dataverse https://doi.org/10.7910/DVN/TI0KAU (2013).
4. Arqueología de La Construcción. vol. I–V (Consejo Superior de Investigaciones Científicas, Instituto de Arqueología, Madrid, 2008).
5. Archeologia del cantiere edile: temi *ed* esempi dall'antichità al medioevo: atti del convegno, Università di Bologna, 21 maggio 2021, *per via telematica*. (All'Insegna del Giglio, Sesto Fiorentino, 2023).
6. Vitruvius Pollio., Granger, F., & British Library. Harley 2767. *On Architecture*. (Harvard University Press, 1931).
7. Pliny & Eichholz, D. E. Natural History, *Volume X*: Books 36-37 [Electronic Resource] Translated by D.E. Eichholz. https://doi.org/10.4159/DLCL.pliny_elder-natural_history.1938 (Harvard University Press, Cambridge, 1962).
8. Artioli, G., Secco, M. & Addis, A. The Vitruvian legacy: mortars and binders before and after the Roman world. in *The Contribution of Mineralogy to Cultural Heritage*. 151–202 https://doi.org/10.1180/EMU-notes.20.4 (Mineralogical Society of Great Britain and Ireland, 2019).
9. Oleson, J. P. et al. The ROMACONS project: a contribution to the historical and engineering analysis of hydraulic concrete in Roman maritime structures. *Int. J. Naut. Archaeol.* **33**, 199–229 (2004).
10. Oleson, J. P. Reconstructing the beginnings of Roman concrete - M. Mogetta 2021. The Origins of Concrete Construction in Roman Architecture: Technology and Society in Republican Italy. Cambridge: Cambridge University Press. Pp. xiv + 311. ISBN 978-1-108-84568-7. *J. Rom. Archaeol.* **36**, 249–257 (2023).
11. DeLaine, J. Production, transport and on-site organisation of Roman mortars and plasters. *Archaeol. Anthropol. Sci.* **13**, 195 (2021).
12. Jackson, M. et al. Extreme durability in ancient Roman concretes. *Am. Ceram. Soc. Bull.* **97**, 22–28 (2018).
13. Leslie, A. B. & Hughes, J. J. Binder microstructure in lime mortars: implications for the interpretation of analysis results. *Q. J. Eng. Geol. Hydrogeol.* **35**, 257–263 (2002).
14. Seymour, L. M., Tamura, N., Jackson, M. D. & Masic, A. Reactive binder and aggregate interfacial zones in the mortar of Tomb of Caecilia Metella concrete, 1C BCE, Rome. *J. Am. Ceram. Soc.* **105**, 1503–1518 (2022).
15. Seymour, L. M. et al. Hot mixing: mechanistic insights into the durability of ancient Roman concrete. *Sci. Adv.* **9**, eadd1602 (2023).
16. Lancaster, L. C. Mortars and plasters—How mortars were made. The literary sources. *Archaeol. Anthropol. Sci.* **13**, 192 (2021).
17. Seymour, L. M., Keenan-Jones, D., Zanzi, G. L., Weaver, J. C. & Masic, A. Reactive ceramic aggregates in mortars from ancient water infrastructure serving Rome and Pompeii. *Cell Rep. Phys. Sci.* **3**, 101024 (2022).
18. Jackson, M. D. et al. Mechanical resilience and cementitious processes in Imperial Roman architectural mortar. *Proc. Natl. Acad. Sci. USA* **111**, 18484–9 (2014).
19. Palomo, A., Monteiro, P., Martauz, P., Bilek, V. & Fernandez-Jimenez, A. Hybrid binders: a journey from the past to a sustainable future (opus caementicium futurum). *Cem. Concr. Res.* **124**, 105829 (2019).
20. Jackson, M. D., Vola, G., Gotti, E. & Zanga, B. Sea-water concretes and their material characteristics. in *Building for eternity: the history and technology of Roman concrete engineering in the sea*. (ed. Oleson, J. P.) 141–188 (Oxbow Books, Havertown, 2014).
21. Jackson, M. D. et al. Cement microstructures and durability in ancient Roman seawater concretes. in *Historic Mortars*. 49–76 https://doi.org/10.1007/978-94-007-4635-0_5 (Springer Netherlands, Dordrecht, 2012).
22. Jackson, M. D. et al. Phillipsite and Al-tobermorite mineral cements produced through low-temperature water-rock reactions in Roman marine concrete. *Am. Mineral.* **102**, 1435–1450 (2017).
23. Elsen, J., Cizer, O. & Snellings, R. Lessons from a lost technology: the secrets of Roman concrete. *Am. Mineral.* **98**, 1917–1918 (2013).
24. Jackson, M. D. et al. Assessment of material characteristics of ancient concretes, Grande Aula, Markets of Trajan, Rome. *J. Archaeol. Sci.* **36**, 2481–2492 (2009).
25. Borno, I. B., Haque, M. I. & Ashraf, W. Crystallization of C-S-H and C-A-S-H in artificial seawater at ambient temperature. *Cem. Concr. Res* **173**, 107292 (2023).
26. Jackson, M. D., Chen, H., Peterson, J. G., Akgul, C. M. & Richards, B. Synchrotron X-ray microdiffraction studies of the mortars of ancient Roman concretes. in *Synchrotron Radiation, Cultural Heritage, Biomineralization*. 203–231 https://doi.org/10.1002/9781394332458.ch7 (2024).
27. Bruni, S. et al. White lumps in fifth-to seventeenth-century AD mortars from Northern Italy. *Archaeometry* **39**, 1–7 (1997).
28. Forster, A. Hot-lime mortars: a current perspective. *J. Archit. Conserv.* **10**, 7–27 (2004).
29. Traini, L. *La Lavorazione Della Calce Dall'antichità al Medioevo: Roma e Le Province Dell'Impero*. (Scienze e Lettere, Roma, 2013).
30. Mogetta, M. The Origins of Concrete Construction in Roman Architecture: Technology and Society in Republican Italy. (Cambridge University Press: Cambridge, 2021).
31. Hufschmid, T. Provincial-sized monumentality: The construction site of the Roman theatre of Augusta Raurica (Switzerland). In *Architectures of the Roman World*. (ed. MUGNAI, N.) 101–122 https://doi.org/10.2307/jj.7657701.12 (Oxbow Books, 2023).
32. Franceschini, M. M. N. et al. Raw materials and building technologies in the public buildings of Pompeii after the earthquake of 62/63 CE: a diachronic analysis of mortars. *Case Stud. Constr. Mater.* **21**, e03943 (2024).
33. Dilaria, S., Previato, C., Secco, M. & Busana, M. S. A semi-automated machine-learning tool for assessing building phases: discriminant analysis of mortars from the 2022 excavation at the sarno bath complex in pompeii. *Heritage* **8**, 51 (2025).
34. Miriello, D. et al. New compositional data on ancient mortars and plasters from Pompeii (Campania – Southern Italy): archaeometric results and considerations about their time evolution. *Mater. Charact.* **146**, 189–203 (2018).

35. Dessales,H. ed. & Amato, V. *Ricostruire dopo un terremoto: riparazioni antiche a Pompei*. (Centre Jean Bérard, Napoli, 2022).
36. Kilian, R., Borgatta, L. & Wendler, E. Investigation of the deterioration mechanisms induced by moisture and soluble salts in the necropolis of Porta Nocera, Pompeii (Italy). *Herit. Sci.* **11**, 72 (2023).
37. Dilaria, S. et al. Phasing the history of ancient buildings through PCA on mortars' mineralogical profiles: the example of the Sarno Baths (Pompeii). *Archaeometry* **64**, 866–882 (2022).
38. Secco, M. et al. Mineralogical clustering of the structural mortars from the Sarno Baths, Pompeii: a tool to interpret construction techniques and relative chronologies. *J. Cult. Herit.* **40**, 265–273 (2019).
39. Scandone, R. & Giacomelli, L. Precursors of eruptions at Vesuvius (Italy). *J. Volcanol. Geotherm. Res.* **171**, 191–200 (2008).
40. Maiuri, A. L'Ultima Fase *Edilizia Di Pompei Con LXVI Tavole Fuori Testo*. (Instituto di Studi Romani, Rome, 1942).
41. Zuchtriegel, G. et al. I cantieri antichi di Pompei tra emergenza e ordinaria manutenzione: nuovi dati dall'Insula 10, Regio IX. (2024).
42. Maragh, J. M., Weaver, J. C. & Masic, A. Large-scale micron-order 3D surface correlative chemical imaging of ancient Roman concrete. *PLoS ONE* **14**, e0210710 (2019).
43. Chu, V., Regev, L., Weiner, S. & Boaretto, E. Differentiating between anthropogenic calcite in plaster, ash and natural calcite using infrared spectroscopy: implications in archaeology. *J. Archaeol. Sci.* **35**, 905–911 (2008).
44. Christensen, J. N. et al. Isotopic fractionation accompanying CO2 hydroxylation and carbonate precipitation from high pH waters at The Cedars, California, USA. *Geochim. Cosmochim. Acta* **301**, 91–115 (2021).
45. Kosednar-Legenstein, B., Dietzel, M., Leis, A. & Stingl, K. Stable carbon and oxygen isotope investigation in historical lime mortar and plaster – results from field and experimental study. *Appl. Geochem.* **23**, 2425–2437 (2008).
46. Vola, G., Gotti, E., Brandon, C., Oleson, J. P. & Hohlfelder, R. L. Chemical, mineralogical and petrographic characterization of Roman ancient hydraulic concretes cores from Santa Liberata, Italy, and Caesarea Palestinae, Israel. *Period. Mineral.* **80**, 317–338 (2011).
47. Graven, H., Keeling, R. F. & Rogelj, J. Changes to carbon isotopes in atmospheric CO2 over the industrial era and into the future. *Glob. Biogeochem. Cycles* **34**, e2019GB006170 (2020).
48. Létolle, R., Gégout, P., Moranville-Regourd, M. & Gaveau, B. Carbon-13 and oxygen-18 mass spectrometry as a potential tool for the study of carbonate phases in concretes. *J. Am. Ceram. Soc.* **73**, 3617–3625 (1990).
49. Miriello, D. et al. Characterisation of archaeological mortars from Pompeii (Campania, Italy) and identification of construction phases by compositional data analysis. *J. Archaeol. Sci.* **37**, 2207–2223 (2010).
50. Loh, H.-C., Kim, H.-J., Ulm, F.-J. & Masic, A. Time-space-resolved chemical deconvolution of cementitious colloidal systems using raman spectroscopy. *Langmuir* **37**, 7019–7031 (2021).
51. Daëron, M. & Vermeesch, P. Omnivariant generalized least squares regression: theory, geochronological applications, and making the case for reconciled δ47 calibrations. Preprint at https://doi.org/10.22541/essoar.169607909.95281327/v1 (2023).
52. Kim, S.-T., O'Neil, J. R., Hillaire-Marcel, C. & Mucci, A. Oxygen isotope fractionation between synthetic aragonite and water: influence of temperature and Mg2+ concentration. *Geochim. Cosmochim. Acta* **71**, 4704–4715 (2007).
53. Bernasconi, S. M. et al. InterCarb: a community effort to improve interlaboratory standardization of the carbonate clumped isotope thermometer using carbonate standards. *Geochem. Geophys. Geosyst.* **22**, e2020GC009588 (2021).

Acknowledgments

We would like to thank the MIT Research Support Committee (RSC) and the MIT Concrete Sustainability Hub (MIT CSHub) for partially funding this research. Furthermore, we thank the MIT Center for Materials Research in Archeology and Ethnology and the DMSE Breakerspace for access to some of the characterization tools used in this study.

Author contributions

Designed research: A.M., J.C.W., and K.B. Performed research: E.V., J.C.W., R.S., V.A., A.R., G.I., and A.M. Contributed new reagents/analytic tools: J.C.W., K.B., and A.M. Analyzed data: E.V., J.C.W., C.H., K.B., C.G., and A.M. Wrote the paper: E.V., J.C.W., and A.M. Reviewed and edited the manuscript: E.V., J.C.W., C.H., K.B., C.G., R.S., V.A., A.R., G.I., G.Z., and A.M.

Competing interests

The authors declare no competing interests.

Additional information

Supplementary information The online version contains supplementary material available at https://doi.org/10.1038/s41467-025-66634-7.

Correspondence and requests for materials should be addressed to Admir Masic.

Peer review information *Nature Communications* thanks Marcello Mogetta and the other anonymous reviewer(s) for their contribution to the peer review of this work. A peer review file is available.